

Autonomous Driving System with a Planar LiDAR-based Localization Method for a Magnetic Wheeled-type Bridge Inspection Robot—BIREM-IV-P

Hyunwoo Song^{*}, Ryota Hatanaka, Masaru Tanida, Yogo Takada

Mechanical and Physical Engineering Graduate School, Osaka City University, Osaka, Japan

Email address:

thgudn@naver.com (H. Song), takada@eng.osaka-cu.ac.jp (Y. Takada)

^{*}Corresponding author

To cite this article:

Hyunwoo Song, Ryota Hatanaka, Masaru Tanida, Yogo Takada. Autonomous Driving System with a Planar LiDAR-based Localization Method for a Magnetic Wheeled-type Bridge Inspection Robot—BIREM-IV-P. *Automation, Control and Intelligent Systems*.

Vol. 9, No. 4, 2021, pp. 111-121. doi: 10.11648/j.acis.20210904.13

Received: November 15, 2021; **Accepted:** December 9, 2021; **Published:** December 24, 2021

Abstract: Since the period of high economic growth, several social infrastructure facilities have been aging. Regular inspections are conducted for safety; however, current bridge inspections are visually performed, which is problematic with regard to cost and safety. Therefore, robots are being considered for inspections. In previous research, a bridge inspection robot was developed, and the small bridge inspection robot BIREM with high driving performance was developed. However, as BIREM-IV is manually operated, autonomous driving is required. In this study, a planar light detection and ranging (LiDAR) sensor, which was developed in the previous study, and a camera was mounted to perform localization for the autonomous driving of the bridge inspection robot BIREM-IV. In addition, in order to mount the sensor necessary for localization in the robot, the driving performance evaluation according to the change of the robot's additional weight and center of gravity was conducted as a previous study, and a new robot was designed and manufactured based on the results. The newly manufactured BIREM-IV-P is path planning by comparing it with the coordinates of the destination point based on the robot's localization information obtained from the mounted planar LiDAR and the camera and analyzes the possibility of autonomous driving to the destination through path tracking.

Keywords: Four-wheel Driving Robot, Bridge Inspection, Planar LiDAR, Autonomous Driving System

1. Introduction

Social infrastructure, which includes bridges and tunnels, is indispensable with regard to support for daily life; however, their functions decline over time. In addition, the social capital stock of Japan is concentrated during the period of high economic growth and is expected to rapidly deteriorate in future. Therefore, national and local governments are conducting periodic inspections to extend the life of bridges. The first inspection will be carried out within 2 years of the development of the bridge and once every 5 years from the first inspection. Current bridge inspections are conducted using scaffolding and specialized vehicles operated by individuals.

Bridge inspections conducted by installing scaffolding are costly and dangerous owing to the development of scaffolds

and working at elevated sites, respectively. In addition, as the number of aging bridges increases, the shortage of inspectors has become a problem. Furthermore, methods using specialized cranes require traffic regulations, which may cause traffic congestion. Therefore, to address the aforementioned problems, robots that inspect bridges are gaining significant attention.

In recent years, several robots, including flying and adsorption types, have been developed to inspect bridges [1-7]. Among these, the adsorption-type robot is always in contact with the inspection environment; thus, it has the advantage of being compatible with the contact-type inspection method. In addition, as energy is not consumed when the robot is stationary, an extended inspection is possible. However, the adsorption-type inspection robot needs to move freely on the bridge surface, namely, moving on a flat plate and shifting

between three-dimensional surfaces.

Therefore, we are developing a bridge inspection robot known as BIREM. Figure 1 shows BIREM-IV, which exhibits a high driving performance; Table 1 demonstrates the specifications [8]. BIREM-IV is a suction-type mobile robot that features a rimless wheel equipped with neodymium magnets; unlike other suction-type robots, it does not require power for suction when it is stopped for bridge inspection. In addition, considering the size of bolts on the bridge between the left and right wheels, it was designed to run on a right-angled path between the front and rear wheels. Therefore, the robot can travel freely under a steel bridge.

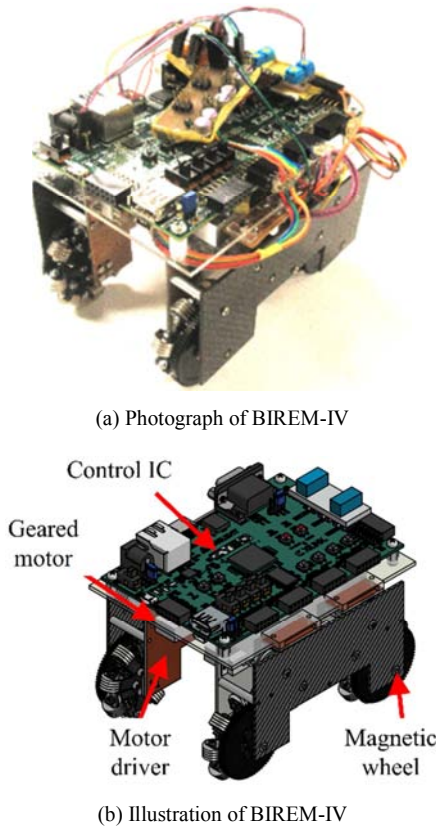


Figure 1. Bridge inspection robot BIREM-IV developed in the previous study.

Table 1. Specifications of BIREM-IV.

BIREM-IV	
Mass	0.487 kg
Size	140.0 mm×102.0 mm×123.0 mm
Control IC	Xilinx Zynq-7000 (XC7Z010-1CLG400C)

BIREM-IV, which was developed for bridge inspection, exhibits a high driving performance. However, this robot is manually operated by a controller, and it is insufficient to solve all the problems considered based on regular visual inspections of an individual. Therefore, it is desirable to make BIREM-IV autonomous. The localization of the robot can be specified by combining the localization method using the planar LiDAR used in the previous study, which used the feature point detection method that includes a camera to improve the accuracy of the localization method. The

autonomous driving experiment was conducted using this method.

2. Bridge Inspection Robot — BIREM-IV-P

A simulation study was conducted to avoid any disruption in traveling when BIREM-IV was weighted with a LiDAR sensor [9]. In this study, based on the experimental results, BIREM-IV-P was redesigned considering the center of gravity. Illustrations and specifications of BIREM-IV-P equipped with necessary sensors and instrumentation equipment for autonomous driving are defined in Figure 2 and Table 2, respectively.

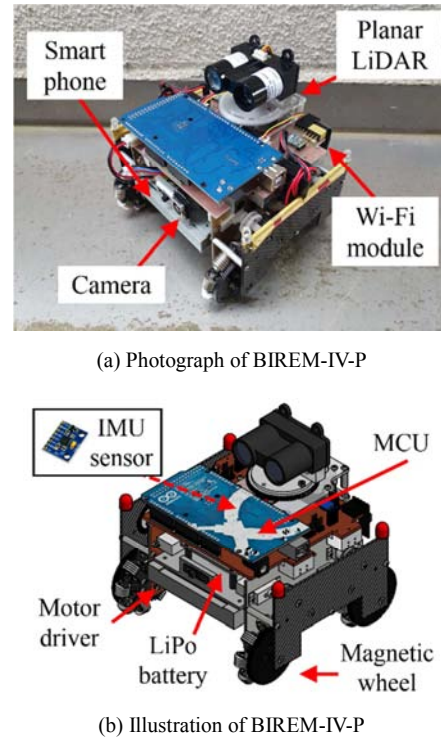


Figure 2. Bridge inspection robot BIREM-IV-P.

Table 2. Specifications of BIREM-IV-P.

BIREM-IV-P	
Mass	0.765 kg
Size	140.0 mm×140.0 mm×135.0 mm
Battery	LiPo, 7.4 V, 1000 mAh, 60C
MCU	Arduino Mega 2560 R3
Controller	Smartphone (Rakuten mini)

Compared with the conventional BIREM-IV, the redesigned BIREM-IV-P does not change its overall size despite being equipped with sensors and instrumentation equipment, and its mass is based on the simulation results in terms of safety, which is within the allowable range. This type of robot performs localization using the mounted planar LiDAR and camera while grasping the direction of the robot and the rotation angle when the coordinate system is converted using the 6-axis IMU sensor.

3. Autonomous Driving Method for BIREM-IV-P

BIREM-IV-P was developed to inspect steel bridges. As the robot functions under a bridge, it cannot receive information from satellites. Therefore, localization cannot be determined using the global navigation satellite system (GNSS) sensor or geomagnetic sensor. In addition, it is impossible to orient itself using geomagnetic sensors owing to magnetic wheels. It is difficult to travel to a destination in the environment under a bridge using the existing localization and autonomous driving methods. Therefore, several studies have used LiDAR sensors to estimate localization and autonomous driving in environments where the GNSS cannot be used. Among these, simultaneous localization and mapping (SLAM), which uses the iterative closest point (ICP) and normal distribution transform (NDT), are used for localization based on the multidimensional LiDAR [10-15]. Estimating the position by collating point clouds using ICP or NDT can accurately determine the location in an environment where GNSS cannot be used. However, these two methods depend on the amount of scanned data.

BIREM-IV-P detects damage at the lower part of a bridge and targets a large structure spanning several hundred meters. Therefore, a simple system was considered to be sufficient for this study while minimizing the amount of data; in the previous study, we estimated localization using a simple system based on the manufactured planar LiDAR, which can help the robot detect objects in all the directions [16].

In addition, to improve the accuracy of the planar LiDAR, the position of the robot can be detected reliably using the image processing results obtained from the camera [17]. The image processing method combines the existing Harris corner detection and Hough transform based on the image captured by the camera and detects the edge located along the moving direction of the robot as a feature point. The feature point is a point where some corners of the lower part of the bridge are set as coordinates using the existing information (design drawings and photos) about the bridge structure.

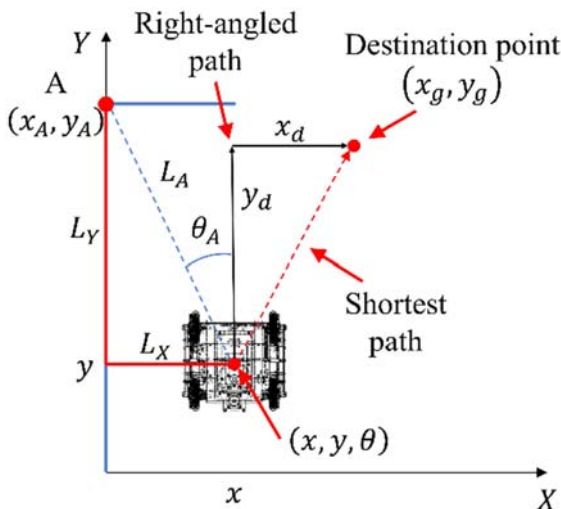


Figure 3. Estimating robot localization and setting the movement path.

Planar LiDAR can localize the robot based on distance and direction data obtained from the feature points. The manufactured planar LiDAR rotates 360° to help the robot detect objects in all the directions and determines the boundary where the distance increases or decreases in the process as a corner point. As shown in Figure 3, localization is performed using the distance from object to the robot and the direction data specific to the robot. Let L_x and L_y be the distances between BIREM-IV-P equipped with the planar LiDAR and a certain feature point A along the X-axis and Y-axis, respectively, which is expressed in (1). In addition, the formula to estimate the position of the robot (as coordinates) is expressed in (2):

$$\begin{aligned} L_x &= L_A \cos(\theta_A) \\ L_y &= L_A \sin(\theta_A) \end{aligned} \quad (1)$$

$$\begin{aligned} x &= x_A + L_x \\ y &= y_A - L_y \end{aligned} \quad (2)$$

where L_A is the distance between the recognized corner and the planar LiDAR, θ_A is the angle indicating the direction from the planar LiDAR to the corner, and x and y denote the coordinates related to the position of the robot. In addition, the position coordinates of the robot are (x, y) , and x_d and y_d , which are the coordinate differences from the position coordinates (x_g, y_g) of the destination point, are defined as follows:

$$\begin{aligned} x_d &= x_g - x \\ y_d &= y_g - y \end{aligned} \quad (3)$$

BIREM-IV-P compares the current location coordinates with the destination location coordinates and performs path planning and path tracking. When a movement path was created, the robot was set to run on a right-angled path to prevent the risk of falling while driving between planes and to pay attention to bolts and nuts under the steel bridge. Therefore, as shown in Figure 3, it creates a right-angled path rather than the shortest path.

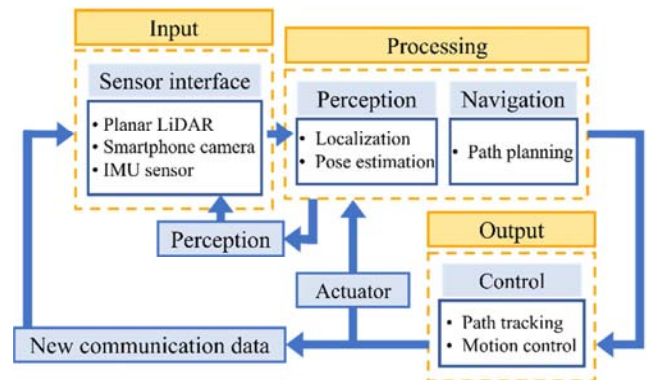


Figure 4. Control flow diagram.

Figure 4 shows the control flow diagram of BIREM-IV-P. The robot detects the feature points using the planar LiDAR

and camera and specifies the direction with the IMU sensor. Then, localization and pose estimation were performed based on the information obtained through these sensors. In this case, the position of the robot was a two-dimensional planar coordinate based on the experimental environment. When the position of the robot is specified, path planning is performed by comparing the current robot position with the coordinates of the destination point. The robot performs path tracking to travel through the path, and at this time, the speed and direction are controlled by changing the PWM of the actuators. In this process, the robot detects the feature point in real time, updates the location information, and checks how far it deviates from the path to control it, so that it does not deviate from the path.

4. Autonomous Driving Experiment

4.1. Traveling Route for Autonomous Driving

In this study, as shown in Figure 5, we developed and experimented with a driving path that can move from the floor to the ceiling through the wall between the surfaces. In the manufactured driving path, a driving area was set using a masking tape to check the movement path and error range of BIREM-IV-P.

BIREM-IV-P starts from the starting point of the prepared experimental environment and moves through points A–C' to the destination. Each path of B–B' and C–C' performs coordinate system transformation from floor to wall and from wall to ceiling, respectively. Finally, the robot moves from point C' to the goal point. In this experiment, corners in each experimental environment were used as feature points, and each feature point was fixed on the plane of each experimental environment. In addition, each feature point has predetermined coordinate position information. The map information used in this autonomous driving is considered assuming that maps are created using other robots, such as those developed in previous research, and existing designs and drawings are used [18].

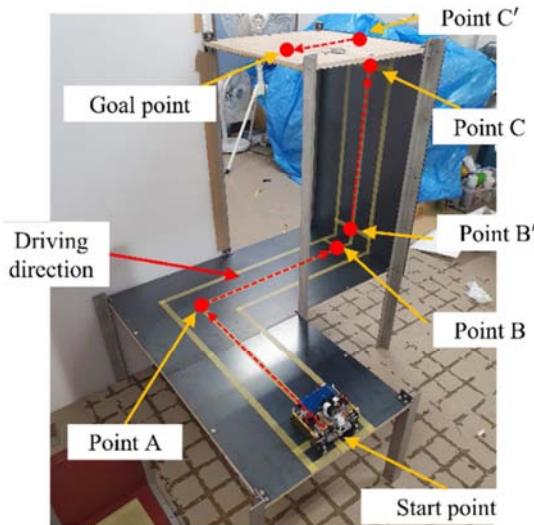
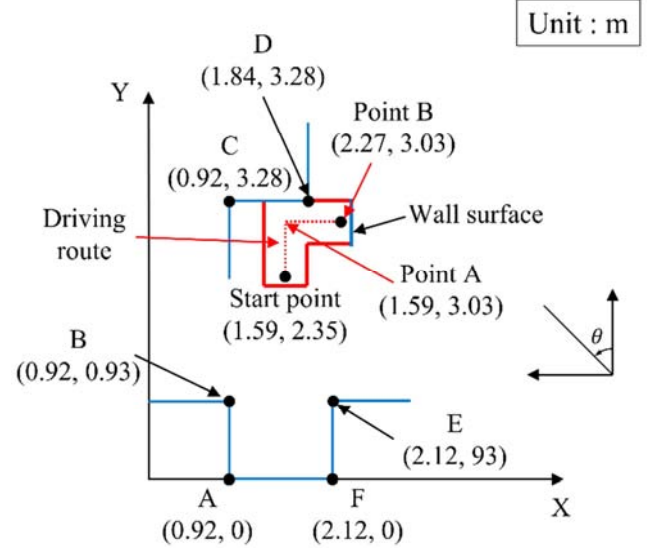
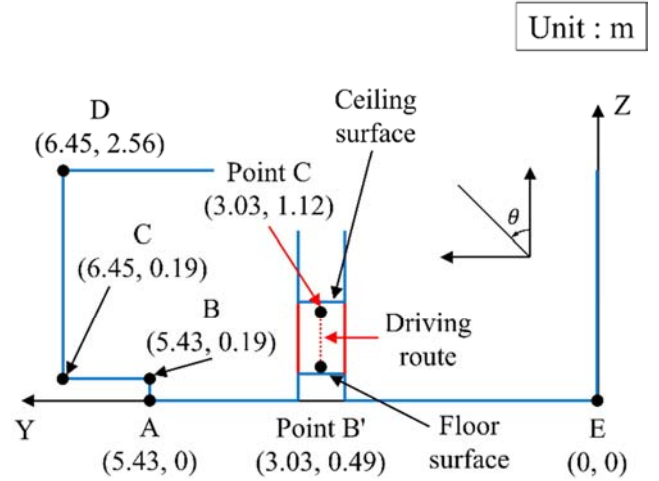


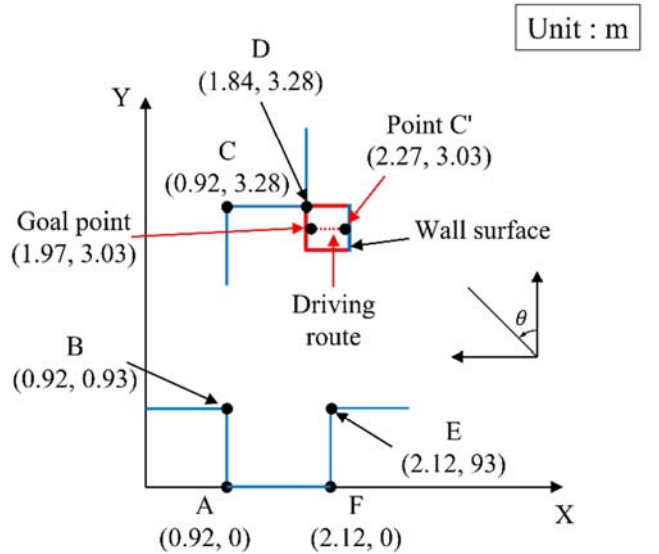
Figure 5. Photograph of experimental environment.



(a) Moving direction and feature point positions when driving on the floor surface



(b) Moving direction and feature point positions when driving on the wall surface



(c) Moving direction and feature point positions when driving on the ceiling surface

Figure 6. Experimental environment.

The localization method based on the planar LiDAR uses two-dimensional data on the plane, and it is difficult to travel to the three-dimensional goal point on the ceiling surface at once. Therefore, in this experiment, the coordinates of points B and B' and points C and C' were set in advance for the passage between the planes, and this was set as the starting point of the coordinate system conversion. The robot passes through each point from A to C' in the process of moving to the destination point and creates a perpendicular path to move to each point. In this process, localization is performed using the information from the feature points in the experimental environment, and autonomous driving is performed from the result to the target point.

The travel area and experimental environment on each running surface are shown in Figure 6(a) for the floor, Figure 6(b) for the wall, and Figure 6(c) for the ceiling. Each corner (the floor and ceiling are from A to F, and the wall is from A to E) of the experimental environment is a known feature point (Figure 6). Each feature point was fixed on the XY plane and had predetermined coordinate position data. Regarding the posture of the robot, θ is defined counterclockwise with $\theta = 0$ (origin) when the robot is facing toward the Y-axis.

4.2. Autonomous Driving on Route 1 (Start Point to Goal Point)

This section includes the experimental results, while the bridge inspection robot BIREM-IV-P moves from the starting point to the goal point. Figure 7 shows the tracking data of the LEDs, which are installed at each corner of the robot, while BIREM-IV-P moves on the floor surface from the starting point to point B.

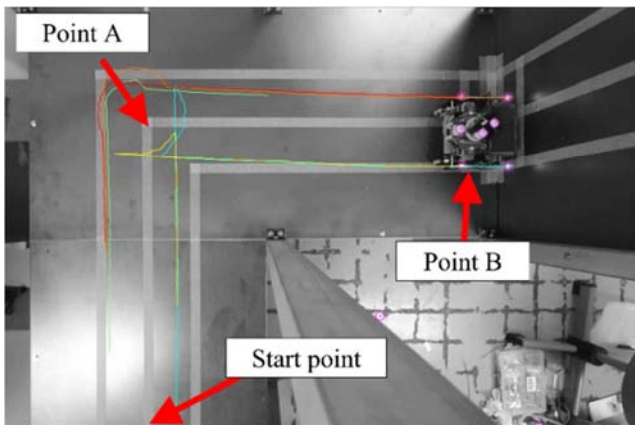


Figure 7. Trajectory of the LED attached to the robot (floor).

Figure 8 shows the motion of BIREM-IV-P on the floor route as time changes. Figures 8(a)–(c) show the movement of the robot from the starting point to point A. Figures 8(c)–(f) show the process of rotating the robot at 90° to move from point A toward point B. Figures 8(f) to (h) show the movement from points A to B.

Figure 9 shows the driving path from the starting point to point B, which was estimated by the planar LiDAR, while BIREM-IV-P moves on the floor.

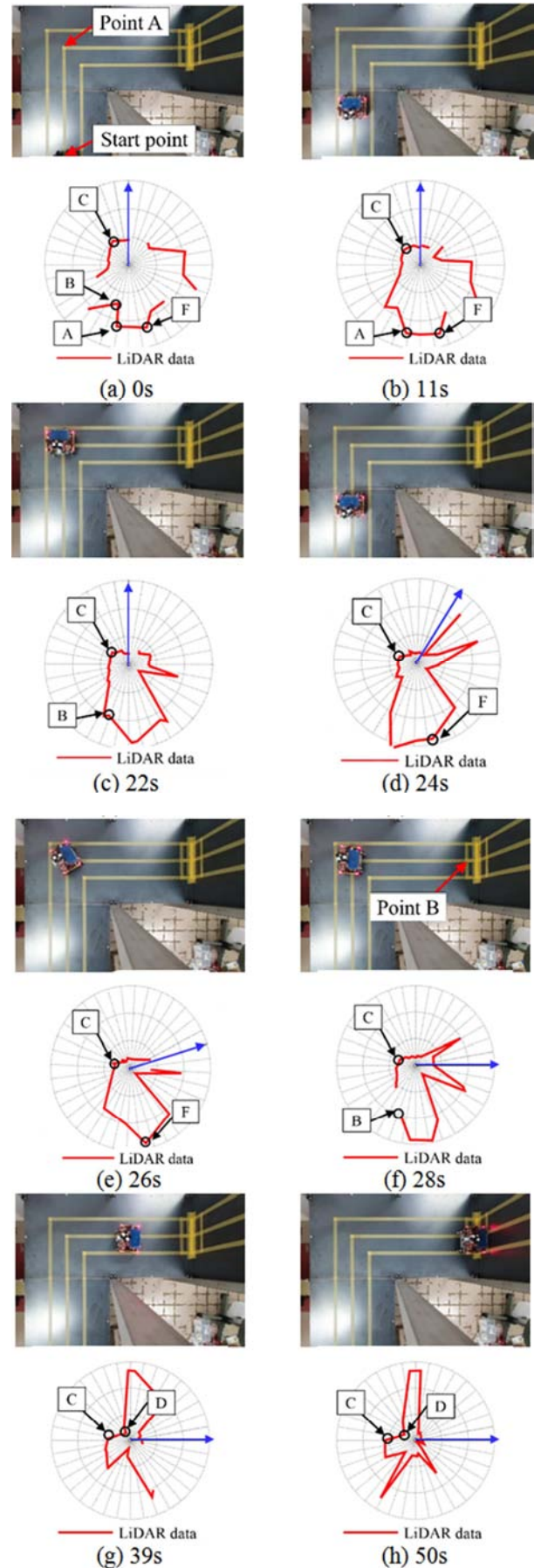


Figure 8. Positional change of robot according to time change (floor).

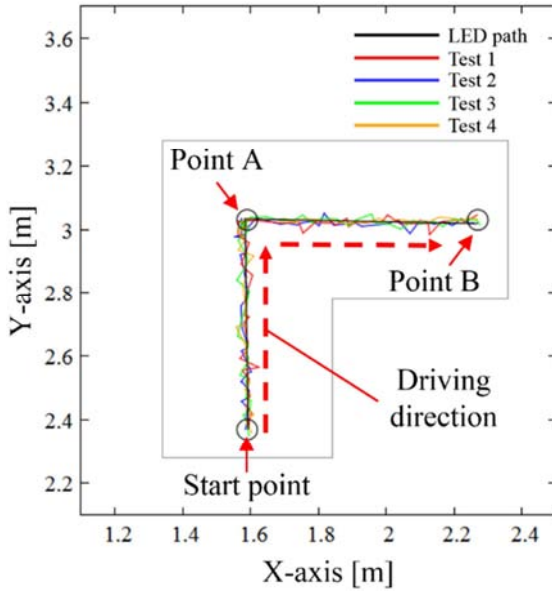


Figure 9. Moving path of BIREM-IV-P using the planar LiDAR-based location information on the floor.

To move from the floor to the wall, the robot that has arrived at point B sets the temporary coordinates of point B' on the wall based on the current location information and moves from the floor to the wall by converting the coordinate system. The process is illustrated in Figure 10.

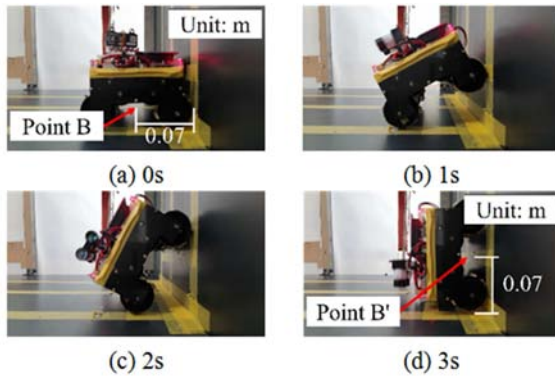


Figure 10. Moving from floor to wall.

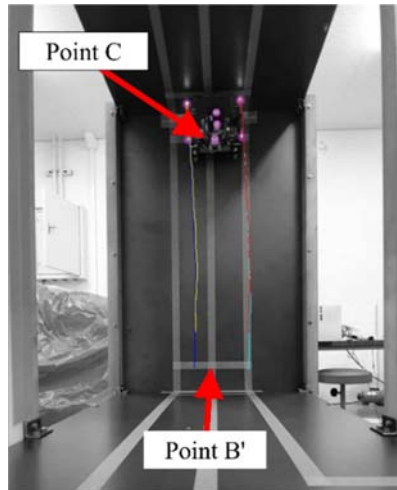


Figure 11. Trajectory of the LED attached to the robot (wall).

As shown in Figure 10(a), the BIREM-IV-P that has arrived at point B, the point where the front wheel of the robot touches the wall and moves toward the temporary coordinate point B'. As shown in Figure 10(d), the plane coordinate system of the robot that has arrived at point B', which is a temporary point where the rear wheel touches the floor, switches from the XY plane to the YZ plane. The robot moves from the floor to the wall through the coordinate system transformation, confirms the location based on localization, and moves to the next passing point, i.e., point C. Figure 11 shows the results of the tracking LEDs that are installed at each corner of the robot, while BIREM-IV-P moves on the wall surface from points B' to C.

Figure 12 shows the movement of BIREM-IV-P on the wall route as time changes. Figures 12(a)–(d) demonstrate the movement of the robot moving from points B' to C.

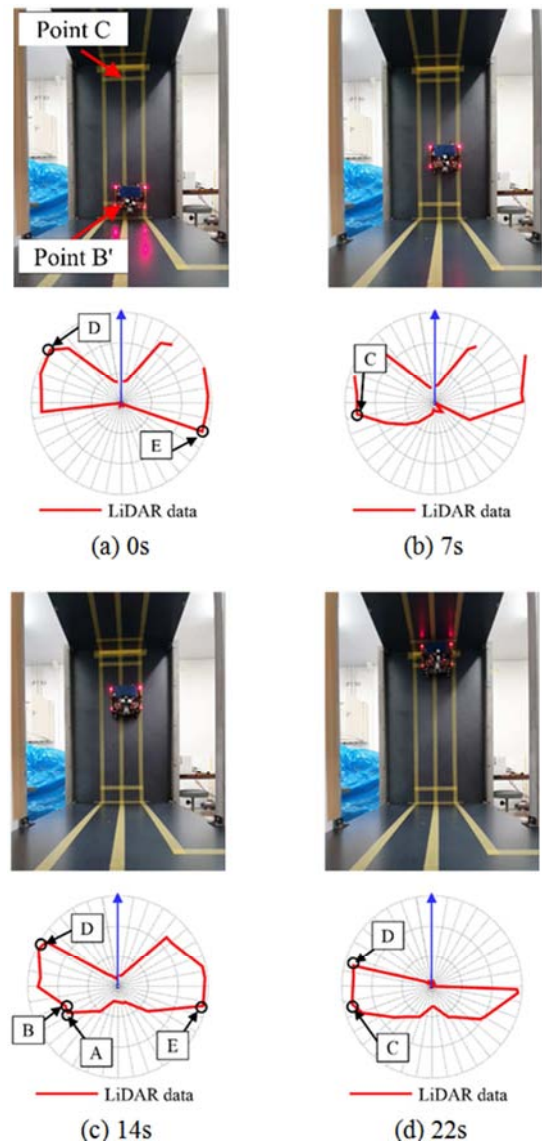


Figure 12. Positional change of robot according to time change (wall).

Figure 13 shows the driving path from points B' to C estimated by the planar LiDAR, while BIREM-IV-P moves on the wall.

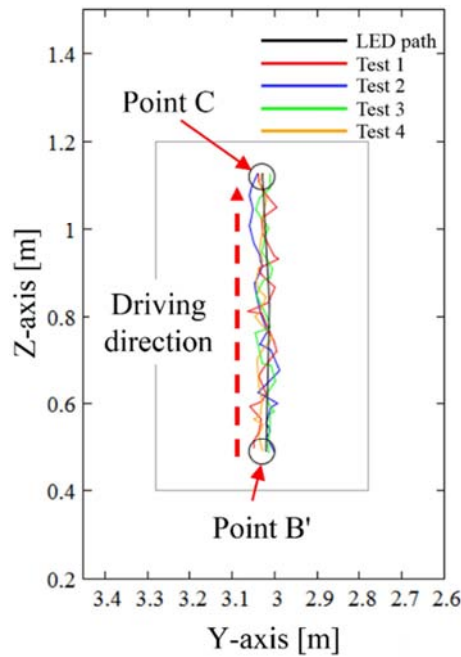


Figure 13. Moving path of BIREM-IV-P using the planar LiDAR-based location information on the wall.

To move from the wall to the ceiling, the robot that has arrived at point C sets temporary coordinates of point C' on the ceiling based on the current location information and moves from the wall to the ceiling by converting the coordinate system. The process is shown in Figure 14.

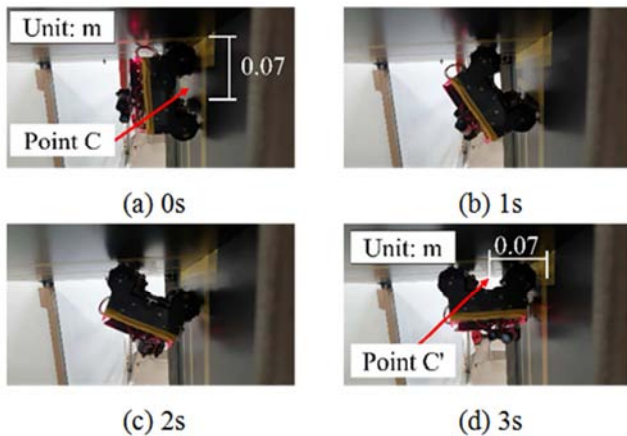


Figure 14. Moving from wall to ceiling.

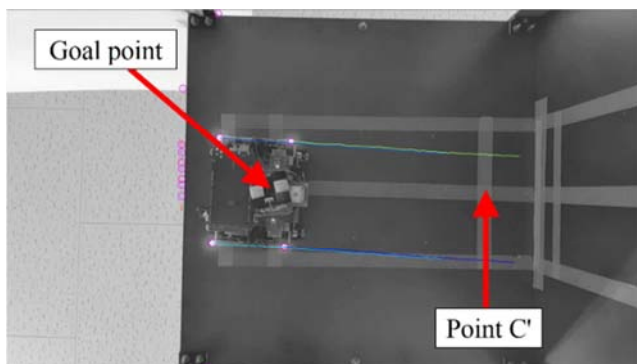


Figure 15. Trajectory of the LED attached to the robot (ceiling).

As shown in Figure 14(a), BIREM-IV-P that has arrived at point C, the point where the front wheel of the robot touches the ceiling, moves toward the temporary coordinate point B'. As shown in Figure 14(d), the plane coordinate system of the robot that has arrived at point C', which is a temporary point where the rear wheel touches the wall, switches from the YZ plane to the XY plane. The robot moves from the wall to the ceiling based on the coordinate system transformation, confirms the location based on localization, and moves to the goal point. Figure 15 shows the results of tracking the LEDs that are installed at each corner of the robot when BIREM-IV-P moves from point C' to the goal point on the floor.

Figure 16 shows the movement path of BIREM-IV-P on the ceiling as time changes. Figures 16(a)–(d) demonstrate the movement of the robot from point C' to the goal point.

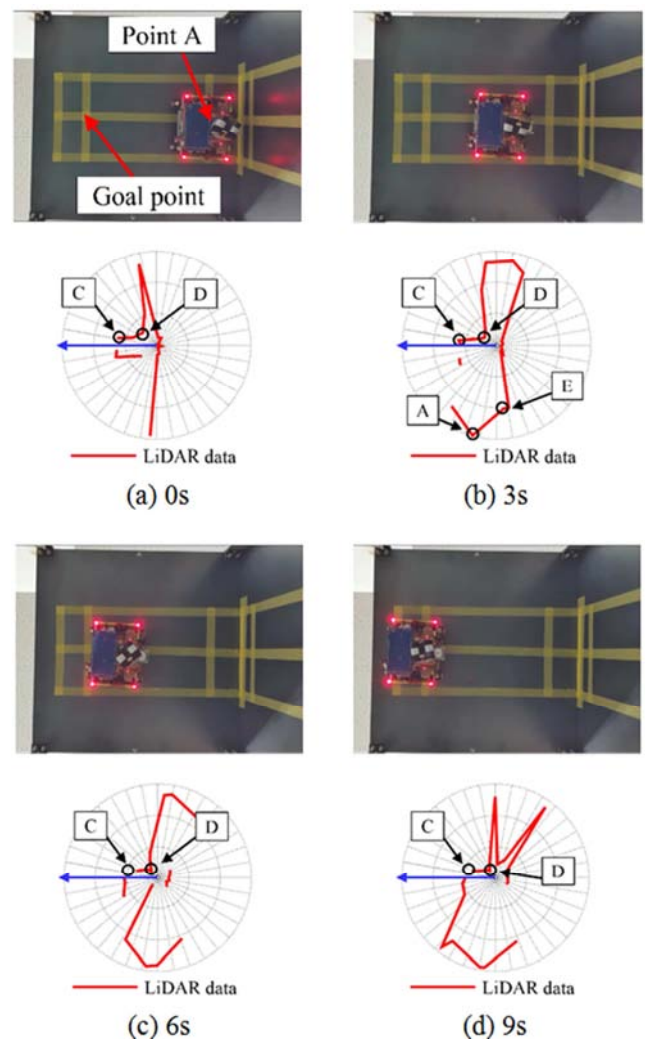


Figure 16. Positional change of the robot according to change in time (Ceiling).

Figure 17 presents the driving path from point C' to the goal point estimated by the planar LiDAR while BIREM-IV-P moves on the ceiling.

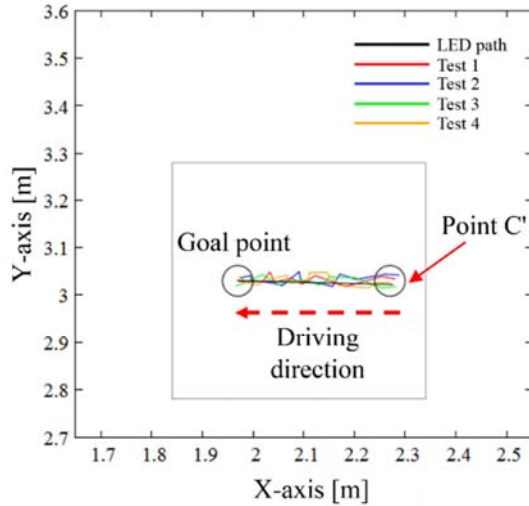


Figure 17. Traveling path of BIREM-IV-P using the planar LiDAR-based location information on the ceiling.

The traveling path from the starting point to the goal point of BIREM-IV-P is shown in Figure 18.

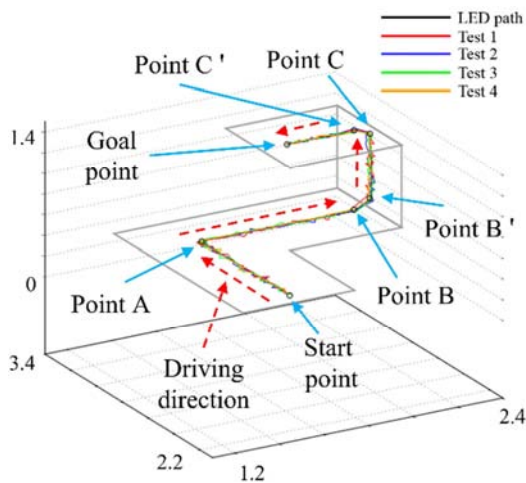
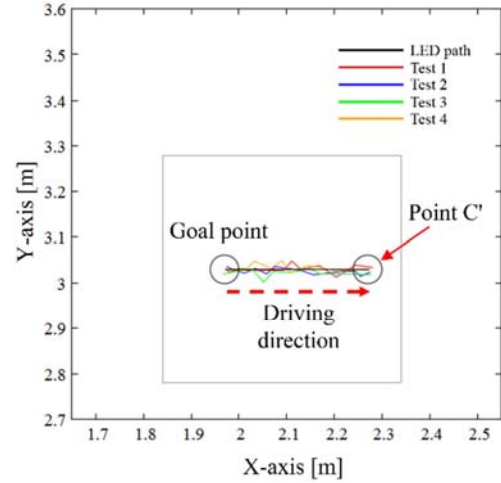


Figure 18. Experimental results of route 1.

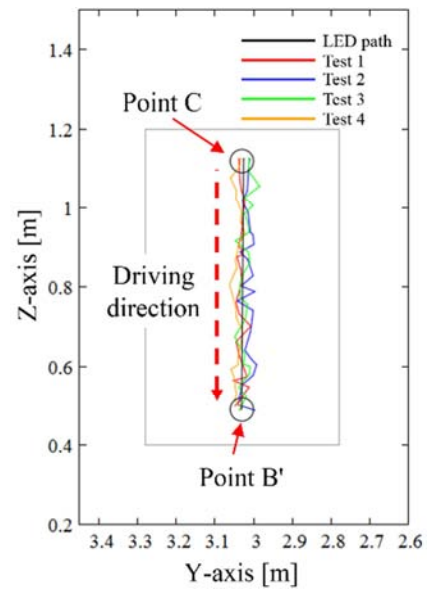
4.3. Autonomous Driving on Route 2 (Goal Point to Start Point)

As a result of the experiment in route 1, it was confirmed that the overall error value increased after the position of the robot was driven between planes. To check whether this is a simple error occurring on each surface or an error caused by running between surfaces, an experiment of route 2 was performed under the same conditions as route 1. In this section, the experimental results are presented, while the bridge inspection robot, BIREM-IV-P, moves from the goal point to the starting point. The robot travels from the goal point to the starting point through each passing point. Figure 19 presents the driving path from the goal point to the starting point estimated by the planar LiDAR when the robot moves in route 2. Figures 19(a)–(c) show the movement paths on the ceiling, wall, and floor, respectively.

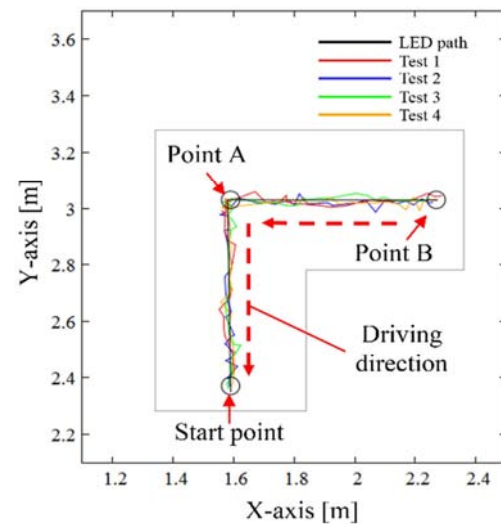
In route 2, the entire travel route from the goal point to the starting point is shown in Figure 20.



(a) Location information on the floor



(b) Location information on the wall



(c) Location information on the floor

Figure 19. Traveling path of BIREM-IV using the planar LiDAR-based location information in route 2.

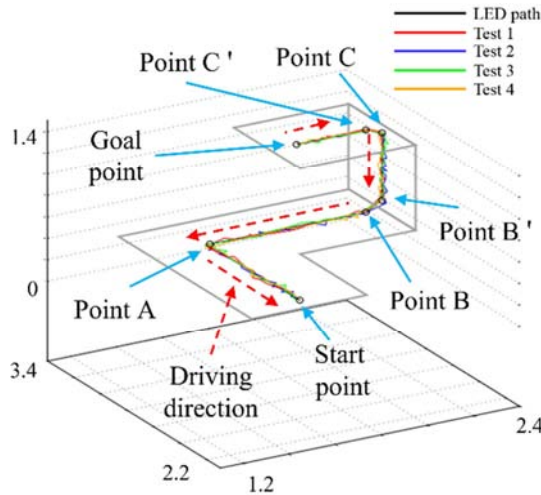


Figure 20. Experimental results of route 2.

4.4. Effect of the Initial State of the Robot and the Position Change of the Passing Point on Movement

This section presents the experimental results of special situations occurring during the movement of BIREM-IV-P. The robot is set to travel on a right-angled path to travel safely from the risk of falling. In other words, the robot rotates 360° in the initial position, and the position coordinates and direction of the robot are set based on the feature point information and direction. At this time, the robot sets the Y-axis of the experimental environment to the 0° point. Therefore, the direction of the robot at the starting point did not affect the experiment.

In addition, an experiment was conducted on the case where the starting point of the robot started at a different location. BIRM-IV-P sets a new passing point between the robot and passing point A if the position of the starting point is changed. As shown in Figure 21, if the robot is placed in a different location and the experiment is conducted, a new path is created by comparing the position of the passing point A and the coordinates of the robot. At this time, the generated path is a right-angled path passing through the virtual passing point V at the point where the difference in the X-or Y-axis between the robot and passing point A becomes 0.

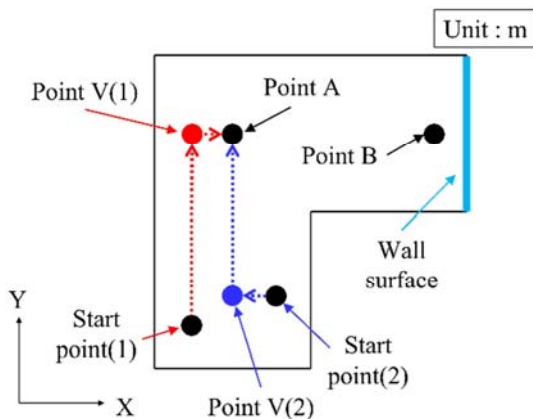


Figure 21. Path planning for traveling to point A from the different start points.

In this way, even if the position of the starting or passing points was set differently, there was no significant impact on the experiment because the route to each passing point was set at right angles for movement. After changing the positions of the starting point and point A of the actual robot, the driving results at point B are shown in Figure 22.

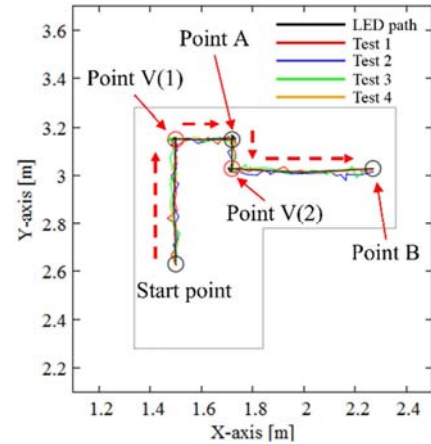
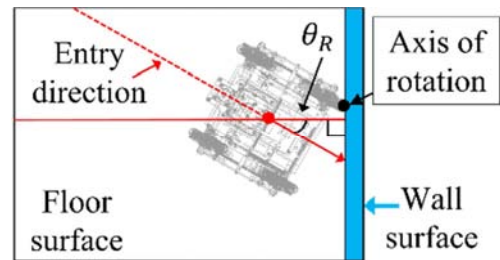
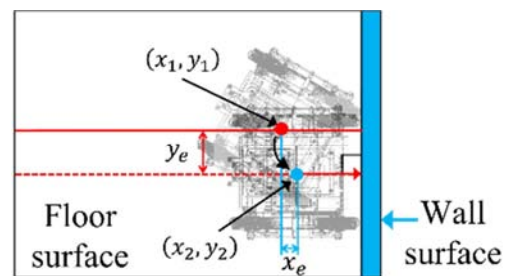


Figure 22. Traveling results when the positions of the starting and passing points are changed.

As shown in Figure 23, an experiment was conducted to analyze the effect of the angle of entry of BIREM-IV-P on the balance of the robot when it travels between surfaces.



(a) Entry angle of the robot when traveling between surfaces



(b) Position error of the robot that occurs during rotation

Figure 23. Effect of the entry angle of the robot with respect to the wall surface on movement.

As a result, as shown in Figure 23(a), when the entry angle θ_R is less than 10° while traveling between surfaces, it rotates to the wall using the first contacted wheel as the rotation axis. As shown in Figure 23(b), two wheels are attached to the front section of the wall, enabling vertical interplane movement. Where 10° , which is the standard for the robot's entry angle, is a result obtained by repeating

inter-plane running experiments and was evaluated based on the entry angle with a running success rate of 100%. Here, when one wheel is rotated as a reference, the center of the robot moves to position B, different from the original position (A), as shown in Figure 23(b), and error values of x_E and y_E occur according to each coordinate.

$$\begin{aligned}x_e &= x_2 - x_1 \\y_e &= y_2 - y_1\end{aligned}\quad (4)$$

As the position error is insignificant, it is not considered to be a major issue.

Table 3. Error in results obtained from the experiment related to route 1.

	Floor surface	Wall surface	Ceiling surface
Minimum error	± 0.19 mm	± 1.36 mm	± 3.54 mm
Maximum error	± 35.04 mm	± 34.52 mm	± 35.12 mm
Average error	± 9.23 mm	± 12.2 mm	± 16.97 mm
Standard deviation	± 7.40 mm	± 8.28 mm	± 8.67 mm

Table 4. Error in results obtained from the experiment related to route 2.

	Floor surface	Wall surface	Ceiling surface
Minimum error	± 2.54 mm	± 0.72 mm	± 0.39 mm
Maximum error	± 42.15 mm	± 41.41 mm	± 28.37 mm
Average error	± 16.39 mm	± 13.12 mm	± 7.87 mm
Standard deviation	± 8.25 mm	± 8.89 mm	± 7.55 mm

As listed in Tables 3 and 4, the average error value increases as the robot moves to the next plane owing to the effect of the additional error value, which occurs when the angle at which the robot enters the next surface increases, as described in the experiment of Section 4.4. However, the lower part of the bridge, which is the actual experimental environment, is thought to be recognizable if the error is within ± 50 mm between the autonomously inspected parts 5 years ago and the newly inspected position. Therefore, the results are within the error range, and the three-dimensional autonomous driving based on the two-dimensional location information and map information proposed in this study is well implemented.

5. Conclusion

BIREM-IV, which inspects the bottom of the bridge, cannot receive data from satellites. Therefore, localization using GNSS is not possible, and autonomous driving becomes complex as the position of the robot is not known. Thus, in this study, we conducted a study on the development of a magnetic bridge inspection robot—BIREM-IV-P—and autonomous driving based on the previously proposed localization method. BIREM-IV-P estimates the current location using the localization method based on the mounted planar LiDAR and camera. Then, by comparing position coordinates of the specified robot with position coordinates of the destination, a driving path is generated to perform autonomous driving. The robot was equipped with sensors, e.g., a planar LiDAR and a camera, necessary for localization. Considering changes in the center of gravity and the mass of

4.5. Experimental Results

As a result of each experiment, BIREM-IV-P traveled past the set passing point to the desired destination. At this time, it was confirmed that autonomous driving to a destination point located in a three-dimensional point was carried out based on two-dimensional information based on the change in the coordinate system while driving between planes and in the plane. In this process, the error values between the actual movement path and the movement path generated based on the location information of the robot specified by the sensors are listed in Tables 3 and 4.

the robot owing to mounted sensors, simulations were performed to evaluate performance, and based on the results, design and development were done.

In this study, an experimental route was prepared to check whether the robot could travel between planes and move from two-dimensional coordinates to the destination of a three-dimensional point; thus, an autonomous driving experiment was conducted. BIREM-IV-P started from the initial point of the floor surface of the created route, transformed the coordinate system from the floor to the wall and from the wall to the ceiling, and then traveled to the destination located on the ceiling. In the process of moving, the robot position obtained using the planar LiDAR and the position of the target point are compared in real time, and the robot moves on the optimum route. At this time, when the bridge inspection robot travels in an environment other than a horizontal surface, such as when traveling between a horizontal plane and a vertical plane, the robot may risk losing its balance and crash if it is not maintained in a horizontal position. Therefore, excluding certain cases, the route is set such that the robot always moves on a right-angled path.

As a result, we estimated the robot's localization in an environment where the GNSS cannot be used to determine a traveling route based on that positional information. It was confirmed that autonomous driving can be safely conducted at the target point.

In future, we will conduct a self-evaluation and simulation to improve the driving performance of robots to inspect bridges and enable travel between walls and more complex routes, e.g., flange route. In addition, we plan to identify

advantages and disadvantages of fusion with odometry using IMU sensors and rotary encoders and obtain reliable positional information data. Moreover, we will aim to specify the position of the robot in three-dimensional coordinates using a one-dimensional long-distance LiDAR sensor. It will be possible to create and move on the best route based on the destination coordinates without setting the positions of points B and C required for the coordinate system transformation in advance.

References

- [1] Mazumdar, A. and Asada, H. H., Mag-Foot: A steel bridge inspection robot, *Intelligent Robots and Systems, IROS 2009 IEEE/RSJ International Conference on 2009* (2009), pp. 1691-1696.
- [2] W. Lee, S. Hirose, Contacting Surface-Transfer Control for Reconfigurable Wall-Climbing Robot Gunryu III, *Journal of Robotics and Mechatronics*, Vol. 25 (2013), No. 3, pp. 439-448.
- [3] Manabu Nakao, Eiji Hasegawa, Taku Kudo, and Naoyuki Sawasaki, Development of a Bridge Inspection Support Robot System Using Two-Wheeled Multicopters, *J. Robot. Mechatron.*, Vol. 31, No. 6 (2019), pp. 837-844.
- [4] Y. Okada, T. Okatani, Development of UAV with Passive Rotating Spherical Shell for Bridge Inspection and its Evaluation of Inspection Capability in Real Bridges, *Journal of the Robotics Society of Japan*, Vol. 34 (2016), No. 2, pp. 119-122 (in Japanese).
- [5] La, H., Dinh, T., Pham, N., Ha, Q., & Pham, A., Automated robotic monitoring and inspection of steel structures and bridges, *Robotica*, Vol. 37, No. 5 (2019), pp. 947-967.
- [6] H. Kajiwar, N. Hanajima, K. Kurashige, Y. Fujihira, Development of Hanger-Rope Inspection Robot for Suspension Bridges, *Journal of Robotics and Mechatronics*, Vol. 31 (2019), No. 6, pp. 855-862.
- [7] Takahiro Ikeda, Kenichi Ohara, Akihiko Ichikawa, Satoshi Ashizawa, Takeo Oomichi, and Toshio Fukuda, Aerial Manipulator Control Method Based on Generalized Jacobian, *J. Robot. Mechatron.*, Vol. 33, No. 2 (2021), pp. 231-241.
- [8] Pang-jo Chun, Ji Dang, Shunsuke Hamasaki, Ryosuke Yajima, Toshihiro Kameda, Hideki Wada, Tatsuro Yamane, Shota Izumi, and Keiji Nagatani, Utilization of Unmanned Aerial Vehicle, Artificial Intelligence, and Remote Measurement Technology for Bridge Inspections, *Journal of Robotics and Mechatronics*, Vol. 32, No. 6 (2020), pp. 1244-1258.
- [9] Hyunwoo Song, Ryota Hatanaka, Yogo Takada, Effects of Centroid Position on Running Performance of Bridge Inspection Robot BIREM-IV, *IOSR Journal of Mechanical and Civil Engineering (IOSR-JMCE)*, Vol. 18, No. 2 (2021), pp. 41-49.
- [10] Tomono, M., A 2-D global scan matching method using euclidean invariant signature, *Journal of the Robotics Society of Japan*, Vol. 25, No. 3 (2007), pp. 390-401 (in Japanese).
- [11] Fumitaka Hashikawa and Kazuyuki Morioka, "Convenient Position Estimation of Distributed Sensors in Intelligent Spaces Using SLAM for Mobile Robots," *J. Robot. Mechatron.*, Vol. 27, No. 2 (2015), pp. 191-199.
- [12] Kiyooki Takahashi, Takafumi Ono, Tomokazu Takahashi, Masato Suzuki, Yasuhiko Arai, and Seiji Aoyagi, "Performance Evaluation of Robot Localization Using 2D and 3D Point Clouds," *J. Robot. Mechatron.*, Vol. 29, No. 5 (2017), pp. 928-934.
- [13] Kanhere, A. V. and Gao, G. X., LiDAR SLAM utilizing normal distribution transform and measurement consensus, *ION GNSS+ 2019* (2019), pp. 2228-2240.
- [14] Tomohiro Umetani, Yuya Kondo, and Takuma Tokuda, Rapid Development of a Mobile Robot for the Nakanoshima Challenge Using a Robot for Intelligent Environments, *J. Robot. Mechatron.*, Vol. 32, No. 6 (2020), pp. 1211-1218.
- [15] R. Mur-Artal and J. D. Tardós, "ORB-SLAM2: An Open-Source SLAM System for Monocular, Stereo, and RGB-D Cameras," in *IEEE Transactions on Robotics*, Vol. 33, No. 5 (2017), pp. 1255-1262.
- [16] Hyunwoo Song, Jun Nakahama, Yogo Takada, Localization method using planar LiDAR for mobile robots to support bridge inspection, *Transactions of the JSME* (in Japanese), Vol. 87, No. 896 (2021), p. 20-00346.
- [17] Hyunwoo Song, Jun Nakahama, Yogo Takada, Localization Method Based on Image Processing for Autonomous Driving of Mobile Robot in the Linear Infrastructure, *Automation, Control and Intelligent Systems*, Vol. 9, No. 1 (2021), pp. 34-45.
- [18] Naoto Imajo, Tomoki Tajiri, Mikiji Kashinoki, and Yogo Takada, Making a three-dimensional map in complicated environment by using a bridge inspection robot with a laser range finder, *Transactions of the JSME* (in Japanese), Vol. 82, No. 833 (2016), pp. 15-00443.